Analysis and Comparison of Notch Filter and Capacitor Voltage Feedforward Active Damping Techniques for LCL Grid-Connected Converters

Rodriguez-Diaz, Enrique; Freijedo, Francisco D.; Vasquez, Juan C.; Guerrero, Josep M.

Published in:
IEEE Transactions on Power Electronics

DOI (link to publication from Publisher):
10.1109/TPEL.2018.2856634

Publication date:
2019

Document Version
Accepted author manuscript, peer reviewed version

This article has been accepted for publication in a future issue of this journal, but has not been fully edited. Content may change prior to final publication. Citation information: DOI 10.1109/TPEL.2018.2856634, IEEE Transactions on Power Electronics

Analysis and Comparison of Notch Filter and Capacitor Voltage Feedforward Active Damping Techniques for LCL Grid-Connected Converters

Enrique Rodriguez-Diaz, *Member, IEEE*, Francisco D. Freijedo, *Senior Member, IEEE*, Juan C. Vasquez, *Senior Member, IEEE*, and Josep M. Guerrero, *Fellow Member, IEEE*.

***Abstract*—The use of LCL filters is a well accepted solution to attenuate the harmonics created by the pulsewidth modulation (PWM). However, inherently LCL filters have a resonance region where the unwanted harmonics are amplified, which can compromise stability. Several techniques have been developed in order to tackle this issue. At first the use of passive damping, by intentionally increasing the resistance of the LCL filter components, is a simple, robust and straightforward solution; however, it decreases the overall efficiency of the system, so in general is unwanted. Alternatively, active damping strategies, where the resonance damping is provided by the current controller, are of major interest. This paper analyses the robustness of the closed-loop dynamics when different active damping techniques are implemented. The analysed active damping techniques, which have been selected because of their readiness and simplicity, are: 1) filtered capacitor voltage feed-forward and 2) second order filters in cascade with the main current controller. The impedance/admittance stability formulation is used to model the system, which has been proven to be very convenient for the assessment of robustness. Experimental tests are provided in order to show the accuracy of the analysis and verify the findings. This paper proves that filtered capacitor voltage feed-forward is more robust and reliable solution than implementations based on cascade notch filters.**

***Index Terms*—Ac/dc converter, active damping, notch filter, current control, converter control, LCL filter, weak grid.**

I. Introduction

Grid-connected voltage source converters (VSC) usually work in current control mode: the PWM voltage reference is obtained from the current error in a closed loop. Current control mode of operation provides features such as peak current control and disturbance rejection. In a cascaded loops control structures, a suitable design guideline points to minimize the time constant of the innermost controllers [1], [2], which in most of the application this role is played by the current controllers. Moreover, fast dynamics are also demanded during faulty/weak grid situation in order to fulfil grid-code requirements [3], [4].

LCL output filters are utilised together with power electronic converters in order to improve the filtering of switching harmonics due to the PWM and fulfil harmonic grid standards. The selection of filter parameters is not a trivial task, since the internal resonance affects to the current controller dynamics [5]–[12]. The objective of damping techniques is to mitigate the LCL filter harmonic amplification around its resonance frequency, which is also related to the closed-loop stability of the system. Passive damping, which intentionally increases the resistance of the LCL components, is in general avoided because decreases the overall efficiency [8], even though is a simple and robust solution.

Active damping techniques, on the contrary, mitigate the effects of the LCL resonance by proper control actions [5], [9]–[11], [13]–[21]; where the use of a filtered capacitor voltage feed-forward [5], [15]–[18] as well as second order notch filters in cascade with the main current controller [21]–[25] are very common approaches, for which the implementation is straightforward.

The use of filtered capacitor voltage feed-forward mimics the capacitor current for the active damping action, since it is estimated by a derivative calculation (i.e., the capacitor current is estimated from a time derivative of the capacitor voltage) [5], [14]–[16]. On the other hand, notch-filters introduce and anti-resonance peak that aims to cancel out the resonance of the LCL filter. The notch is typically placed at the resonance frequency of the LCL filter [21], [23], [25] and the damping of the poles and zeros are used to determine the depth and width of the notch. A different approach is to place the anti-resonance peak of the notch filter separated from the expected LCL resonance frequency, in order to account for possible resonance frequency drifts due to change in the physical parameters [22]. Furthermore, an alternative strategy to systematically re-tune the notch filter for the resonance frequency measured on-site by signal injection methods [25]. This latest implementation is far more complex, nevertheless, it can effectively avoid frequency drifts created by the ageing of passive elements.

Overall, the chosen structures are convenient because of their readiness and simplicity, since they require minor modifications of the controllers implementation without needing any extra sensor. In practice, the use of filtered capacitor voltage feed-forward does not require extra-sensors, since the capacitor voltage is already measured for grid synchronization. On the other hand notch filters are simply cascaded to the main controller. At first, the notch filter approach seems more intuitive, but some drawbacks such as sensitivity to

Manuscript received March 28, 2017; revised May 6, 2017 and April 25, 2018; accepted June 29, 2018.

Enrique Rodriguez-Diaz, Juan C. Vasquez and Josep M. Guerrero are with the Department of Energy Technology, Aalborg University, 9220 Aalborg East, Denmark. E-mails: {erd,juq,joz}@et.aau.dk.

Francisco D. Freijedo, is with the Power Electronics Lab, Ecole Polytechnique Federale de Lausanne, CH1015, Lausanne Switzerland. E-mail: francisco.freijedo@epfl.ch.

This article has been accepted for publication in a future issue of this journal, but has not been fully edited. Content may change prior to final publication. Citation information: DOI 10.1109/TPEL.2018.2856634, IEEE Transactions on Power Electronics

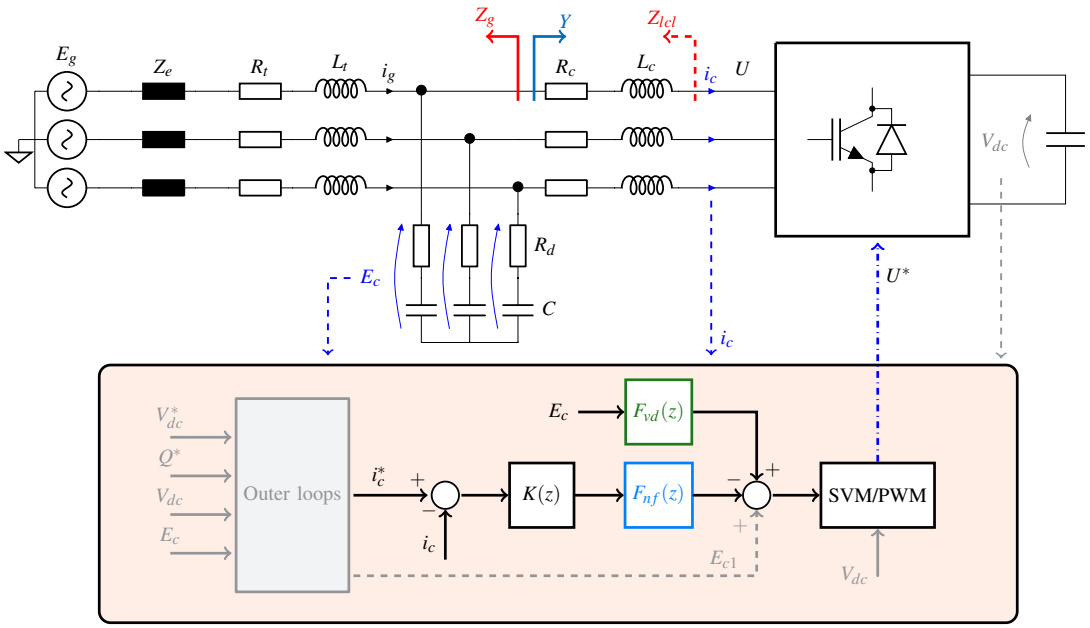

Fig. 1: Current control of LCL grid-connected VSC converter.

frequency deviations is reported [25]. However, literature lacks of a comprehensive and systematic comparison between both basic techniques. Therefore, the motivation of this paper is to provide such a comprehensive comparison in terms of dynamic response, disturbance rejection, harmonics mitigation and overall stability.

The impedance/admittance formulation is used to solve the control problem. Analytical expressions for the derivation of the grid impedance and converter admittances, as a function of the system parameters, are presented. Theoretical assessments of stability, disturbance rejection, and robustness (i.e. uncertainty of grid impedance value) for both current controller structures, are provided. Subsequently, a set of representative experimental tests are provided, which includes: 1) current reference step change, 2) voltage dips, 3) response evaluation in weak grid conditions.

The rest of the paper is organised as follows. Section II describes the system of the LCL grid-connected converter, and the current controllers for the different active damping approaches. Section III provides the design methodology of the current controller. Section IV shows the theoretical comparison of the designed current controllers. Section V describes the lab-scale prototype used for the experimental verification, and the tests carried out to verify the findings. Finally the paper is concluded by summarizing the main findings and contribution.

II. System Description and Methodology

A. Circuit Modelling

Fig. 1 represents a LCL grid-connected VSC working in current control mode. The stiff grid voltage, point of connection and VSC voltage are represented by E, E_c and U respectively. The LCL filter is formed by a transformed leakage inductance, filter capacitance and the converter side inductor. Both inductors are modelled as an inductance with a series resistance L_c and R_c for the converter side inductor, and L_t and R_t for the transformer leakage inductance and resistance. The capacitor filter is modelled by a capacitance with a series resistance, named C_p and R_p respectively. The voltage across the capacitors is used as the point of connection for the impedance/admittance formulation. The external grid impedance is represented by $Z_e(j\omega)$, which depends on power system circuit and grid conditions [11], [26]. From the inverter point of view, the full-grid impedance ($Z_g(j\omega)$) is dominated by the transformer leakage inductance (L_t); but under weak-grid conditions when $Z_e(j\omega)$ is non-negligible.

Furthermore, Fig. 1 shows the current controller structures for both active damping strategies, where $K(z)$ is the main current controller, $F_{vd}(z)$ and $F_{nf}(z)$ the two analysed damping actions, which shape the converter admittances [15], [27].

B. Current Controller Structure

As shown in Fig. 1 there are two main controller structures that will be analysed, where only one of the active damping actions, $F_{vd}(z)$ (filtered capacitor voltage feed-forward) or $F_{nf}(z)$ (cascaded notch filters) will be used at a time. In both structures, the main controller, which in this work is a proportional-resonant (PR) controller, implemented in $\alpha\beta$-frame with k_p and k_i being the proportional and resonant gains, ω_1 the fundamental frequency, and $T_s = 2\pi/\omega_s$ the controller sampling period.

$$K(z) = k_p \; + \; k_i T_s \frac{1 - cos(\omega_1 T_s) z^{-1}}{1 - 2cos(\omega_1 T_s) z^{-1} + z^{-2}} \qquad (1)$$

The control action includes a feed-forward path that provides a filtered value of the voltage at the point of connection (cf. E_{c1} in Fig. 1) in order to improve the initial transient. [27].

This article has been accepted for publication in a future issue of this journal, but has not been fully edited. Content may change prior to final publication. Citation information: DOI 10.1109/TPEL.2018.2856634, IEEE Transactions on Power Electronics

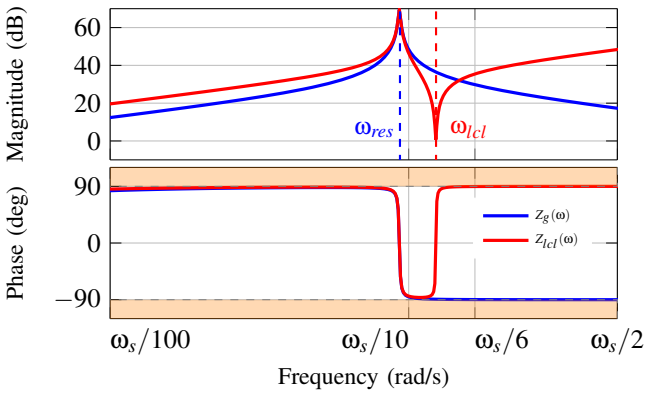

Fig. 2: Impedances comparison. Frequency response of $Z_g(\omega)$ and $Z_{lcl}(\omega)$.

C. LCL filter

The transformer leakage inductance imposes the hardware design in many relevant grid-connected applications, such as wind turbines. In practice, L_t is set by the transformer leakage. Typical values for the secondary inductance are then in the range [0.06, 0.1] p.u: (wind turbine rated power is used for base calculations) [15].

Following LCL design basic guidelines, the secondary inductance also constraints the selection of the converter filter: a primary inductance equal to the transformer inductance is a reasonable design to optimize the switching harmonics filtering [5], [6]. For transformer-less applications, the design rule that considers $L_t = L_c$ is also a reasonable to optimize filtering of PWM harmonics. Therefore, using L_t as an input constraint, in practice, the main degree of freedom of the LCL filter is the choice of the capacitance C. The rated LCL resonance frequency (angular) is

$$\omega_{lcl} = \sqrt{\frac{L_t + L_c}{L_t L_c C}}. \tag{2}$$

The selection of ω_{lcl} involves a trade-off between control interactions and filtering [5]. For active damping, typical values at which the capacitor voltage feedback is more effective are in the range [$0.1\omega_s$,$0.2\omega_s$] [5].

As shown in Fig. 1, if the inverter side current is used as feedback, the LCL filter is split in two parts, on one side the converter side inductor, formed by L_c and R_c, is included in the converter admittance, while the capacitor branch (C_p and R_p) and the grid side inductor (L_t and R_t) are modelled as part of the grid impedance, $Z_g(j\omega)$. The explicit derivation is given as follows

$$Z_g(j\omega) = Z_{gp}(j\omega) /\!/ Z_{gs}(j\omega) \tag{3}$$

where

$$Z_{gp}(j\omega) = \frac{1 + R_p C_p j\omega}{C_p j\omega} \tag{4}$$

and

$$Z_{gs}(j\omega) = L_t j\omega + R_t + Z_e(j\omega) \tag{5}$$

with

$$\omega_{res} = \sqrt{\frac{1}{(L_t + L_e)C}} \tag{6}$$

being the resonance frequency of $Z_g(\omega)$.

D. Active Damping Actions

Two different active damping actions are modelled in this work.

1) Filtered Capacitor Voltage Feed-forward: The use of the filtered capacitor voltage includes a feed-forward path defined as

$$F_{vd}(z) = k_{ad} C \frac{1 - z^{-1}}{T_s} \tag{7}$$

where k_{ad} is the active damping gain, and C the nominal value of the LCL filter capacitor. The discrete time implementation, based on the Backward-Euler rule, provides a dominant derivative action only for frequencies below $0.2\omega_s$; however, in practise $\omega_{lcl} < 0.2\omega_s$ is a quite reasonable assumption to the hardware design constraint [6], [15]. Alternatively, the non-ideal generalized integrators have been proposed for scenarios with higher ω_{lcl} [16]. Therefore, this implementation is also considered in the analysis, as shown in Section III-A.

2) Notch Filter: For active damping actions based on cascaded filters, notch filter provide higher robustness and resonance damping than other second-order filter topologies [5], [21], [22], [24]. The notch filter in the z-domain can be defined as

$$F_{nf}(z) = \frac{A_2 z^{-2} + A_1 z^{-1} + A_0}{B_2 z^{-2} + B_1 z^{-1} + B_0} \tag{8}$$

with,

$$A_2 = 4 - 4\omega_{nf}\xi_z T + \omega_{nf}^2 T_s^2 \tag{9}$$
$$A_1 = -8 + 2\omega_{nf}^2 T_s^2 \tag{10}$$
$$A_0 = 4 + 4\omega_{nf}\xi_z T + \omega_{nf}^2 T_s^2 \tag{11}$$
$$B_2 = 4 - 4\omega_{nf}\xi_p T + \omega_{nf}^2 T_s^2 \tag{12}$$
$$B_1 = -8 + 2\omega_{nf}^2 T_s^2 \tag{13}$$
$$B_0 = 4 + 4\omega_{nf}\xi_p T + \omega_{nf}^2 T_s^2 \tag{14}$$

where ω_{nf} is the anti-resonance peak frequency, and ξ_p and ξ_z are the damping factor of the poles and zeros, respectively [for the physical discrete implementation, the gains of (14) are normalized: all the gains in (14) are divided by B_0].

E. Grid Impedance and Converter Admittances

The admittance/impedance formulation is used to analyse and assess the robustness of the current controllers with different active damping actions for LCL grid-connected converters. The main advantage of this approach is to disaggregate the effect of changes in the grid impedance and the controller structure, which eases the study of the different active damping techniques. The use of converter-side current as feedback signal is implicit in the conventional impedance/admittance modelling [7], [14], [27].

Fig. 3 shows the z-domain model of the system in Fig. 1. The z-domain expression have been obtained by considering

This article has been accepted for publication in a future issue of this journal, but has not been fully edited. Content may change prior to final publication. Citation information: DOI 10.1109/TPEL.2018.2856634, IEEE Transactions on Power Electronics

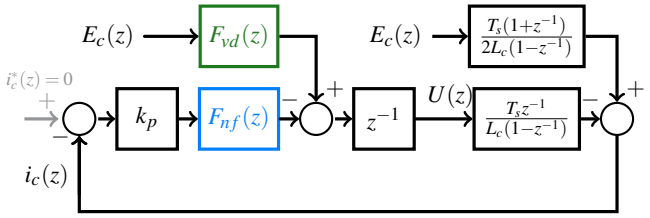

Fig. 3: Model of Current control of LCL grid-connected VSC converter in Z-domain.

the sample and hold effects in the discretization of the plant: the ZOH method has been used to discretize the elements that drive into the discrete device, meanwhile the Tustin method is more accurate to represent the effects on the plant due to the disturbance $Ec(z)$ [3], [28], [29].

$$P_{zoh}(z) = \frac{T_s z^{-1}}{L_c(1-z^{-1}) + R_c T_s z^{-1}} \tag{15}$$

$$P_{tustin}(z) = \frac{T_s(1+z^{-1})}{2L_c(1-z^{-1}) + R_c T_s(1+z^{-1})}. \tag{16}$$

The converter admittance defines the relation between the converter current $i_c(z)$, and the voltage at the point of connection $E_c(z)$. The explicit derivations of $Y(z)$ for the current controllers, with and without active damping, are obtained from Fig. 3, and the expressions are as follows

$$Y(z) = \left.\frac{i_c(z)}{E_c(z)}\right]_{i_c^*=0} \tag{17}$$

$$Y_{wo}(z) = \frac{P_{tustin}(z)}{1 + k_p z^{-1} P_{zoh}(z)} \tag{18}$$

$$Y_{vd}(z) = \frac{P_{tustin} - F_{vd}(z) z^{-1} P_{zoh}(z)}{1 + k_p(z) z^{-1} P_{zoh}(z)} \tag{19}$$

$$Y_{nf}(z) = \frac{P_{tustin}(z)}{1 + k_p F_{nf}(z) z^{-1} P_{zoh}(z)} \tag{20}$$

where $Y_{wo}(z)$ is the converter admittance of the current controller without active damping, $Y_{vd}(z)$ is the converter admittance for the filtered capacitor voltage feed-forward strategy, and $Y_{nf}(z)$ is the converter admittance when the cascade notch filter implementation is used.

Ideally, in order to achieve perfect disturbance rejection, and fast and damped dynamics, the converter admittance would be shaped, with proper control structures and control gains tuning, to be $|Y(j\omega)| \approx 0$ at all frequencies. In practise this cannot be achieved, since it corresponds to an infinite bandwidth. However, it is expected that the active damping techniques improve the disturbance rejection at the critical frequencies, e.g., by reducing $|Y_{vd}(j\omega)|$ and $|Y_{nf}(j\omega)|$ when $\omega \approx \omega_{res}$.

By analysing (18) it can be derived that for low frequencies, i.e., when $z \approx 1$, $|Y_{c-wo}(z)| = 1/(R_c + k_p) \approx 1/k_p$, while at higher frequencies $|Y_{wo}(z)| \approx T_s/L_c(z-1)$. The same conclusions can be derived from (19) and (20). Therefore, the active damping actions do not modify the converter admittance neither at low or high frequencies. Then, as shown in section III, the design goals should focus on shaping $Y_{vd}(j\omega)$ and $Y_{nf}(j\omega)$ to reduce dynamic interactions with $Z_g(j\omega)$ around the potential values of ω_{res}.

F. Formulation for the Current Controllers Assessment

The Impedance/Admittance stability formulation is used in this work, in order to assess the robustness of the closed loop system. After the derivation of the converter admittances and grid impedance, the closed-loop dynamics are set by the interaction between these two components [27], as shown in

$$i_c(z) = \frac{1}{1 + Y(z) Z_g(z)} \left[G_c(z)\ i_c^*(z) \ +\ Y(z)\ E_c(z) \right]. \tag{21}$$

It should be remarked that $Y(z)$ is a function of the interface filter in combination with the controller transfer functions. The effect of outer loops, such as phase-locked loop, dc-link or reactive power control, in $Y(z)$, can be neglected, as in practice the bandwidth of those outer loops should be much smaller than ω_{res} [30]–[33]. Using a similar reasoning, the path providing $E_c 1$, which improves the grid-connection initial transient [see Fig. 1], can be also neglected [27]. The impedance/admittance stability formulation can be also used to design the current controllers. As shown in [15], an optimal tuning, of the current controller using filtered capacitor voltage feed-forward, is obtained by the root-locus examination of the sensitivity function, defined by $S(z) = 1/[1 + Y(z) Z_g(z)]$ [see (21)].

In [15], the optimal tuning is calculated as the solution to the optimization problem that maximizes the real part of the dominant poles of a sensitivity function defined in the s-domain; i.e., placing the dominant poles the furthest from the unstable region. However, in this work the analysis has been performed in the z-domain, in order to obtain a better approximation of the system delays. Therefore, in the z-domain, the objective is to place the dominant poles the furthest away from the unity circle (i.e. unstable region), or in other words, to minimize the dominant poles radius.

III. Design of the Current Controllers

The theoretical approach and the current controllers tuning, have been based on the lab-scale prototype used for experimental verification. Table I shows the physical parameters employed for analysis and experimental verification.

It is clear that variations of the nominal parameters (i.e. switching frequency, filter parameters) would required a re-tuning of the current controllers, for instance, as seen in [12], k_p and k_{ad} are highly dependent on the filter inductances and filter capacitor, respectively. Furthermore , the notch filter is tuned for a specific resonance frequency, therefore a change in the filter parameters requires a re-tune of the notch filter as well.

However, since a key aspect of the analysis is to show how the different active damping actions change the closed loop dynamics, a relatively low resonance frequency is selected [5]. In fact, this is a correct hardware design in the sense that the converter gradually losses control action abilities at high frequencies. As explained in section II, $Z_e(s)$ is neglected

This article has been accepted for publication in a future issue of this journal, but has not been fully edited. Content may change prior to final publication. Citation information: DOI 10.1109/TPEL.2018.2856634, IEEE Transactions on Power Electronics

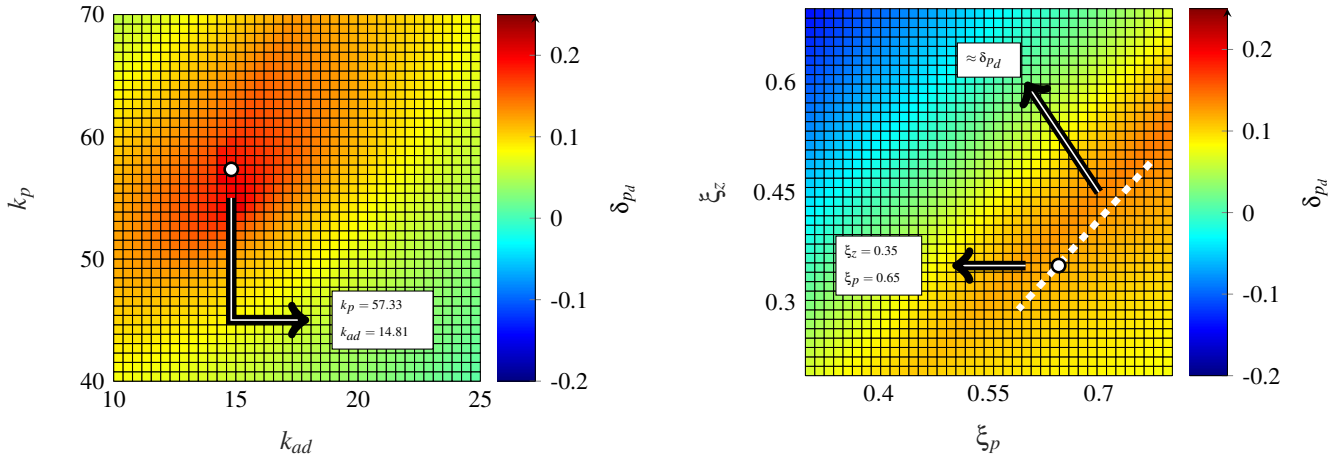

Fig. 4: Results of the direct search, which shows the distance of the dominant poles of $S(z)$ to the unstable region. (a): $k_p - k_{ad}$ plane for the capacitor voltage feed-forward implementation. (b): $\xi_z - \xi_p$ plane for the notch filter implementation.

at rated conditions, since $|Z_e(s)| << |L_t s + R_t|$ is an accurate assumption. Specially for low power scale circuits, because the leakage inductance of the transformer is much higher than other impedances in the path of the stiff grid.

In order to make a fair comparison between the two different active damping techniques, the main current controllers is designed for the same theoretical closed loop bandwidth (i.e. same k_p).

A. Design of Current Controller with Filtered Capacitor Voltage Feed-forward

A robust tuning procedure for the current controller using the filtered capacitor voltage feed-forward has been already presented [15], where the optimal tuning is obtained when placing the dominant poles of $S_{vd}(s)$ the furthest away from the stability region (i.e. right-hand plane), by maximizing the $|\Re(p_{d_{\pm j}})|$. Since, in this work the z-domain has been used during the modelling stage, the distance, of the dominant poles to the unity circle, has been maximized [$\delta_{p_d} = 1 - |p_{d_{\pm j}}|$, see Fig. 5(b)], which for the parameters of the lab-scale prototype gives $k_p = 57.33,\ k_{ad} = 14.81$. Fig. 4(a) shows the results of the direct search method for the controller gains tuning.

Fig. 5 show a comparison of different implementations of the derivative action. The discrete time implementation based on the Backward-Euler rule provides an accurate magnitude match while the phase match degrades for frequencies above $0.2\omega_s$. On the other hand, non-ideal generalized integrators (GI) provide a more accurate phase match for a longer frequency range, but at the cost of increasing the magnitude for frequencies above $0.2\omega_s$. This magnitude mismatch create a resonance in the converter admittance, as shown in Fig. 5(c). The resonance is avoided if the damping parameter of the non-ideal GI (i.e. ω_c in [16]) is increased enough, so the frequency response well matches the one with the Backward-Euler implementation. Therefore, from the admittance shape, both the well damped GI and the Backward-Euler implementations have a best overall performance and both are equally suitable.

B. Design of Current Controller with Notch Filter

Different design criteria, for the selection of the notch filter parameters, have been discussed in the literature [21], [22]. An intuitive design criterion would be to place the notch filter at the resonance frequency ($\omega_{nf} = \omega_{res}$, being ω_{res} the resonance frequency of Z_g), in order to cancel out the resonance peak, meanwhile ξ_z and ξ_p set the width and the depth of the notch. A robust design is achieved when the width of the notch is selected to account for possible deviations of the resonance frequency [21], [23], [25]. Then ξ_z and ξ_p are selected to account for a 10% resonance frequency deviation ($\Delta\omega = 0.1\omega_{res}$) and an attenuation in the frequency range of $\omega_{res} \pm \Delta\omega$ equal to the resonance peak (cf. $a_\Delta = a_{peak}$ and $a_{\omega f} = 2a_\Delta$ in [21]). Applying this methodology the resulting current controller parameters are $k_p = 57.33$, $\xi_z = 0.02$, $\xi_z = 0.3$, and $\omega_{nf} = \omega_{res}$, for an attenuation at the resonance frequency of $a_{\omega f} \approx 20dB$. This configuration is referred as "high attenuation" tuning in the rest of the paper.

A different approach is presented in [22], where the notch filter is designed for a $\omega_{notch} \neq \omega_{res}$ to account for the frequency deviation caused by changes in the LCL filter parameters. This method uses the phase boost provided by the notch filter to stabilize the current control, when the resonance frequency of the LCL filter is place above $f_s/6$. Nevertheless this strategy could also provide higher robustness in weak grid conditions, when the LCL resonance frequency decreases. In order to perform a fair comparison, 10% resonance frequency deviation ($\Delta\omega = 0.1\omega_{res}$) has also been considered as design objective. Following the design guidelines provided in [22], The filter parameters are $\xi = 3$, $\lambda = 1$ and the rejection bandwidth $\Omega = 2\pi 500\ rad/s$. This configuration is named "phase lead" tuning.

Alternatively, the tuning methodology shown in Section III-A, which well fits the impedance/admittance formulation, has been also used for the selection of the notch filter coefficients. First, it has been found that placing the notch filter at the resonance frequency, of grid impedance, maximizes

This article has been accepted for publication in a future issue of this journal, but has not been fully edited. Content may change prior to final publication. Citation information: DOI 10.1109/TPEL.2018.2856634, IEEE Transactions on Power Electronics

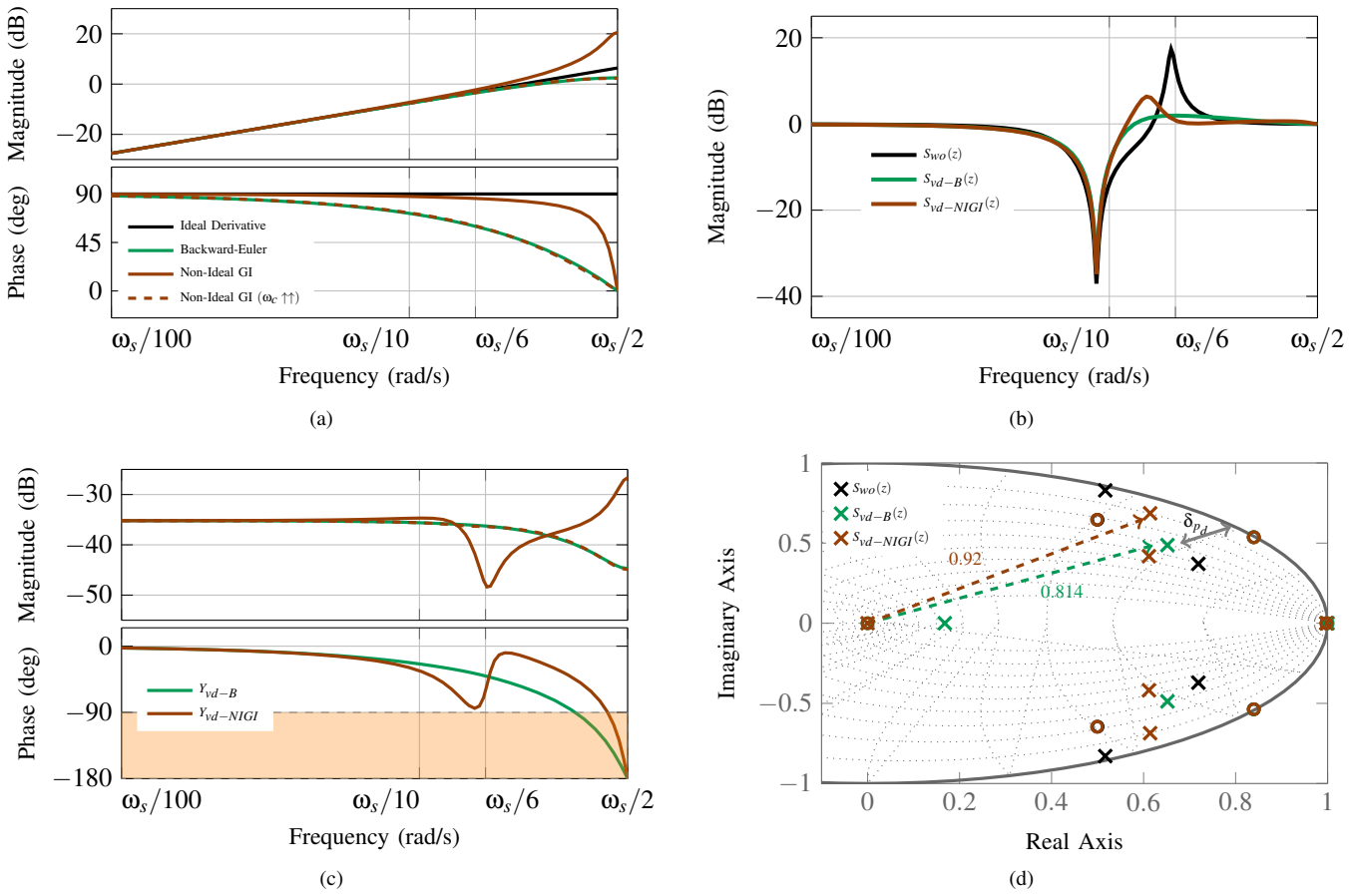

Fig. 5: Effect of derivative implementations. (a) Frequency response of the derivative actions. (b) Frequency response of $Y_{vd}(z)$. (c) Frequency response of $S_{vd}(z)$. (d) Root-loci of $S_{vd}(z)$.

stability for any reasonable set of ξ_z and ξ_p. Then, by a direct search analysis, a set of ξ_z and ξ_p, that maximizes the relative stability, has been found. The direct search results are shown in Fig. 4(b), and the controller parameters are as follows: $k_p = 57.33$, $\xi_z = 0.3$, $\xi_z = 0.65$, and $\omega_{nf} = \omega_{res}$. This configuration is named "robust" notch tuning.

In Fig. 6 the tunings of the current controllers, using a cascaded notch filter, are compared. In Fig. 6(b), it can be seen that all tunings reduce the sensitivity peak of $S_{nf}(z)$, therefore increasing the stability margin of the closed loop system [1]. Fig. 6(c) shows that the "robust" notch tuning has the higher stability margin since the dominant poles of $S_{nf}(z)$ are placed further away from the unstable region.

Furthermore, in Fig. 6(a), the "high attenuation" and "phase lead" tuning shows a peak in the frequency response of $Y_{nf}(j\omega)$ for frequencies slightly below ω_{res}, worsening the disturbance rejection and reducing the passivity compliance region. This is due to the low damping used for the zeros of the notch filters, since it can be seen that a more damped solution (i.e. "robust tuning") has a smoother frequency response.

IV. Comparison Between the Two Active Damping Techniques

In this section, a comparison of the active damping implementations, based on the filtered capacitor voltage feed-forward and cascaded notch filters, is presented.

A. Dynamic Response and Stability

A comparison of the two implementations that have shown the highest stability margins within the different active damping approaches, backward-euler based capacitor voltage feed-forward and the "robust" tuning notch filter, are shown in Fig. 7.

In general sensitivity functions can be used to assess the stability of the closed-loop system. On one side, low maximum sensitivity peaks in $S_m(\omega)$ relate to a good relative stability margin [1], [29]; therefore, as seen in Fig. 7(b), both active damping techniques effectively reduce the sensitivity peak, bringing the system to a more stable position, while the backward-euler based capacitor voltage feed-forward approach provides the highest stability margin.

This trend can be also observed in Fig. 7(c), where the dominant poles of $S_{vd-B}(z)$ are the furthest away from the the unity circle (unstable region).

Furthermore, the dynamic response can be assessed from the position of the dominant poles shown in Fig 7(c). The further away the dominant poles are from the unity circle, the faster and more damped dynamic response. Therefore, it is expected that the filtered capacitor voltage feed-forward approach offers a better dynamic response as well.

This article has been accepted for publication in a future issue of this journal, but has not been fully edited. Content may change prior to final publication. Citation information: DOI 10.1109/TPEL.2018.2856634, IEEE Transactions on Power Electronics

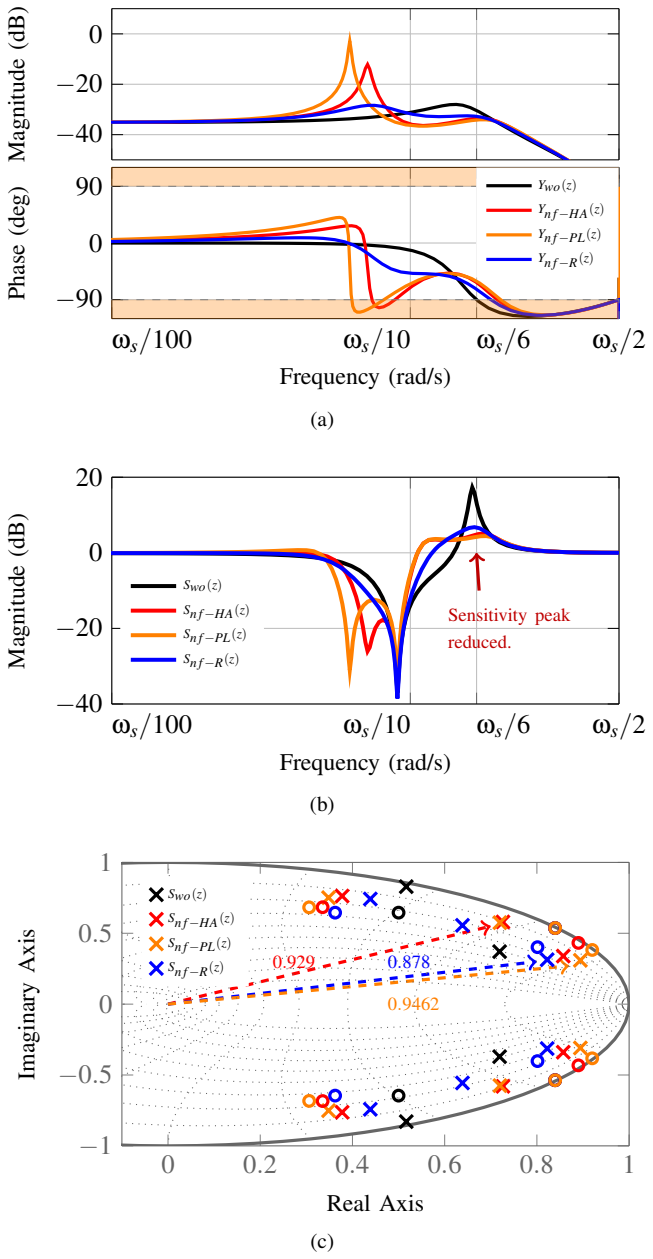

Fig. 6: Frequency response and root-loci of the system with no active damping (black), and with cascade notch filter active damping for the "high attenuation" (red), "robust" tunings (blue), and "phase lead" tuning (orange). (a) Frequency Responses of converter admittances, $Y_{nf}(z)$. (b) Frequency response of sensitivity functions, $S_{nf}(z)$. (c) Root-loci of sensitivity functions, $S_{nf}(z)$.

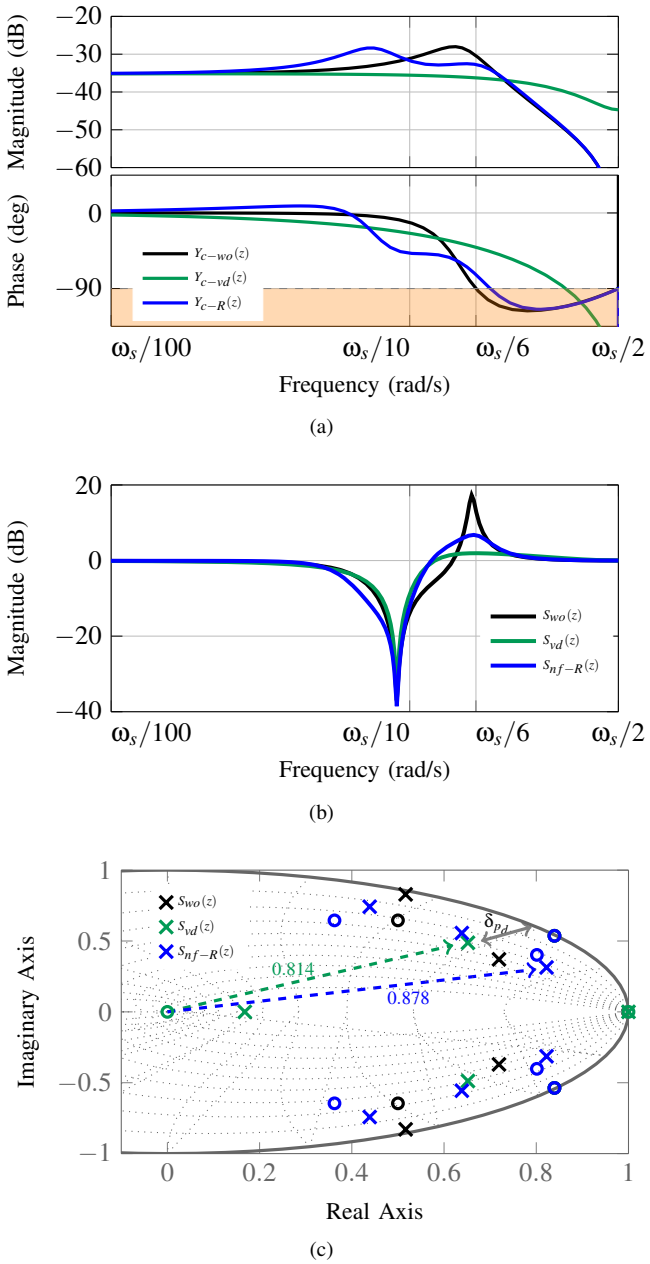

Fig. 7: Frequency response and root-loci of the system with no active damping (black) with cascade notch filter (blue), and filtered capacitor voltage feed-forward (green) active damping actions. (a) Frequency responses of converter admittances, $Y(z)$. (b) Frequency response of sensitivity function, $S(z)$. (c) Root-loci of sensitivity function, $S(z)$.

Furthermore, δ_{pd} can also be employed as a measure of robustness. Therefore, it is easily appreciated that again, the filtered capacitor voltage feed-forward approach offers higher robustness, when variations in the parameters of the physical system are expected [34], [35].

B. Robustness against Weak Grid Conditions

Variations of the physical system may compromise the stability, since current controller are generally tuned for a nominal physical system. This is specially critical in the implementation based on the notch filter, since with the notch filter is intended to cancel out the resonance frequency of the grid impedance. In practise, the external grid impedance, represented by $Z_e(\omega)$ in Fig. 1, can vary significantly, since it depends on the grid conditions [11], [26].

During the design stage, in section III, $Z_e(j\omega)$ has been neglected, because in normal conditions the grid impedance is dominated by the transformer leakage inductance. However,

This article has been accepted for publication in a future issue of this journal, but has not been fully edited. Content may change prior to final publication. Citation information: DOI 10.1109/TPEL.2018.2856634, IEEE Transactions on Power Electronics

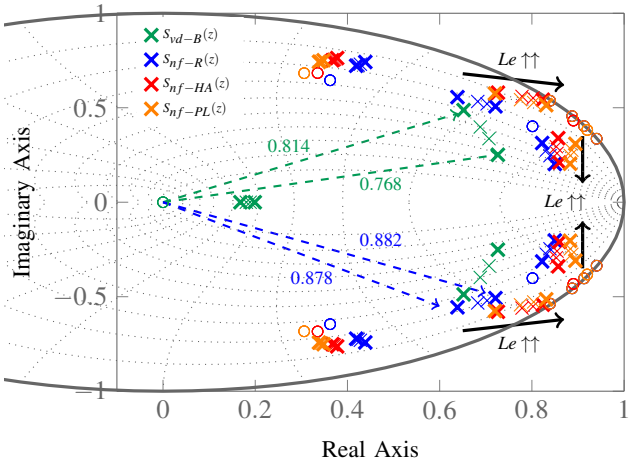

(a)

Fig. 8: Root-loci comparison of the sensitivity functions $S(j\omega)$ in the presence of a L_e increment from 0 to 0.2 p.u.

under weak grid conditions, i.e. when $Z_e(j\omega)$ increases (inductive behaviour has been considered, $Z_e(j\omega) = L_e j\omega$), the full grid impedance $Z_g(j\omega)$ is modified, therefore affecting the resonance frequency [ω_{res} of $Z_g(j\omega)$], and the closed loop dynamics. In order to assess this effect, a sensibility analysis for the grid impedance is performed for the different active damping approaches.

It is expected that the system that has the highest stability margin, in nominal conditions, would be the more robust against variation in the physical system. Fig. 8 shows the effect of a L_e variation, from 0 to 0.2 p.u., on the dominant poles of $S_{nf}(j\omega)$ and $S_{vd}(j\omega)$ for different tunings. While the dominant poles of $S_{nf}(j\omega)$ move towards the unstable region for all analysed tunings, especially for the "high attenuation" and "phase lead" tuning, the dominant poles of $S_{vd}(j\omega)$ move away from the unity circle to a more stable position. This result also predicts a much higher robustness of the capacitor voltage active damping technique.

C. Converter Admittance and Disturbance Rejection Capability

By inspecting the converter admittances magnitude, it can be appreciated that the filtered capacitor voltage feed-forward approach, based on the Backward-Euler implementation, improves the disturbance rejection capability around the critical frequencies ω_{res} and $\omega_s/6$, since the $|Y_{vd}(j\omega)|$ is significantly smaller.

Also, it is interesting to notice that the converter admittance of the current controller with the filtered capacitor voltage feed-forward $[Y_{vd}(j\omega)]$ predicts a passive behaviour up to $\omega_s/3$, while the notch filter approach might significantly reduce the passive region, as seen in Fig. 6(a). This is an important feature, since the interest on design for passivity methodologies for grid-connected VSCs have grown due to the drastical increase of power electronics in renewable energy applications [14], [36]. As an example, input admittance passivity compliance is a requirement in traction standards [37], [38].

Table I: Physical System Parameters

Parameter	Value
Rated Power	$S = 2.2\,\text{kVA}$
Rated Voltage (Line to line RMS)	$V = 400\,\text{V}$
Converter inductance	$L_c = 8.6\,\text{mH}(0.123\,\text{p.u.})$
Converter equivalent resistance	$R_c = 0.27\,\Omega(0.012\,\text{p.u.})$
Capacitor	$C_p = 4.5\,\text{uF}(0.039\,\text{p.u.})$
Capacitor ESR	$R_p = 1\,\text{m}\Omega(< 0.001\,\text{p.u.})$
Grid Side Inductance	$L_t = 4.7 + 1.8 = 6.5\,\text{mH}(0.097\,\text{p.u.})$
Grid Side Resistor	$R_t = 0.22\,\Omega(0.010\,\text{p.u.})$
Study Case 1	
Switching frequency	$f_s = 10\,\text{kHz}$
$F_{vd-B}(z)$	$\frac{6.667\ 10^{-05}z - 6.667\ 10^{-05}}{0.0001z}$
$F_{vd-NIGI}(z)$	$\frac{1.185z^2 - 0.2615z - 0.9239}{z^2 + 1.558z + 0.6065}$
$F_{nf-HA}(z)$	$\frac{0.7359z^2 - 1.2236z + 0.7163}{z^2 - 1.2236z + 0.4524}$
$F_{nf-PL}(z)$	$\frac{0.8363z^2 - 1.455z + 0.8347}{z^2 - 1.455z + 0.671}$
$F_{nf-R}(z)$	$\frac{0.8803z^2 - 1.248z + 0.601}{z^2 - 1.248z + 0.4813}$
Study Case 2	
Switching frequency	$f_s = 7.5\,\text{kHz}$
$F_{vd-B}(z)$	$\frac{8.8\ 10^{-05}z - 8.889\ 10^{-05}}{0.0001333z}$
$F_{vd-NIGI}(z)$	$\frac{1.143z^2 - 0.3226z - 0.8208}{z^2 + 1.433z + 0.5134}$
$F_{nf-HA}(z)$	$\frac{0.69z^2 - 0.999z + 0.6671}{z^2 - 0.999z + 0.3571}$
$F_{nf-PL}(z)$	$\frac{0.8011z^2 - 1.249z + 0.7991}{z^2 - 1.249z + 0.6001}$
$F_{nf-R}(z)$	$\frac{0.8027z^2 - 1.073z + 0.6548}{z^2 - 1.073z + 0.4575}$

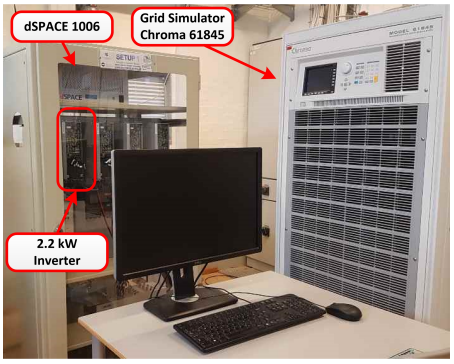

Fig. 9: Experimental test-bed

V. Experimental Results

Table I shows the physical parameters employed for the analysis and experimental verification. The theoretical analysis has shown that the use of the filtered capacitor voltage feed-forward for active damping offers higher relative stability and robustness, and a better disturbance rejection, when compared to the approach with a cascaded notch filters. In order to verify the findings, the different current controller structures have been tested in test-bed shown in Fig. 9.

Fig. 10 shows the grid current $i_c(t)$ for current steps commands of 5A (100% of converter's rated power) and for voltage

This article has been accepted for publication in a future issue of this journal, but has not been fully edited. Content may change prior to final publication. Citation information: DOI 10.1109/TPEL.2018.2856634, IEEE Transactions on Power Electronics

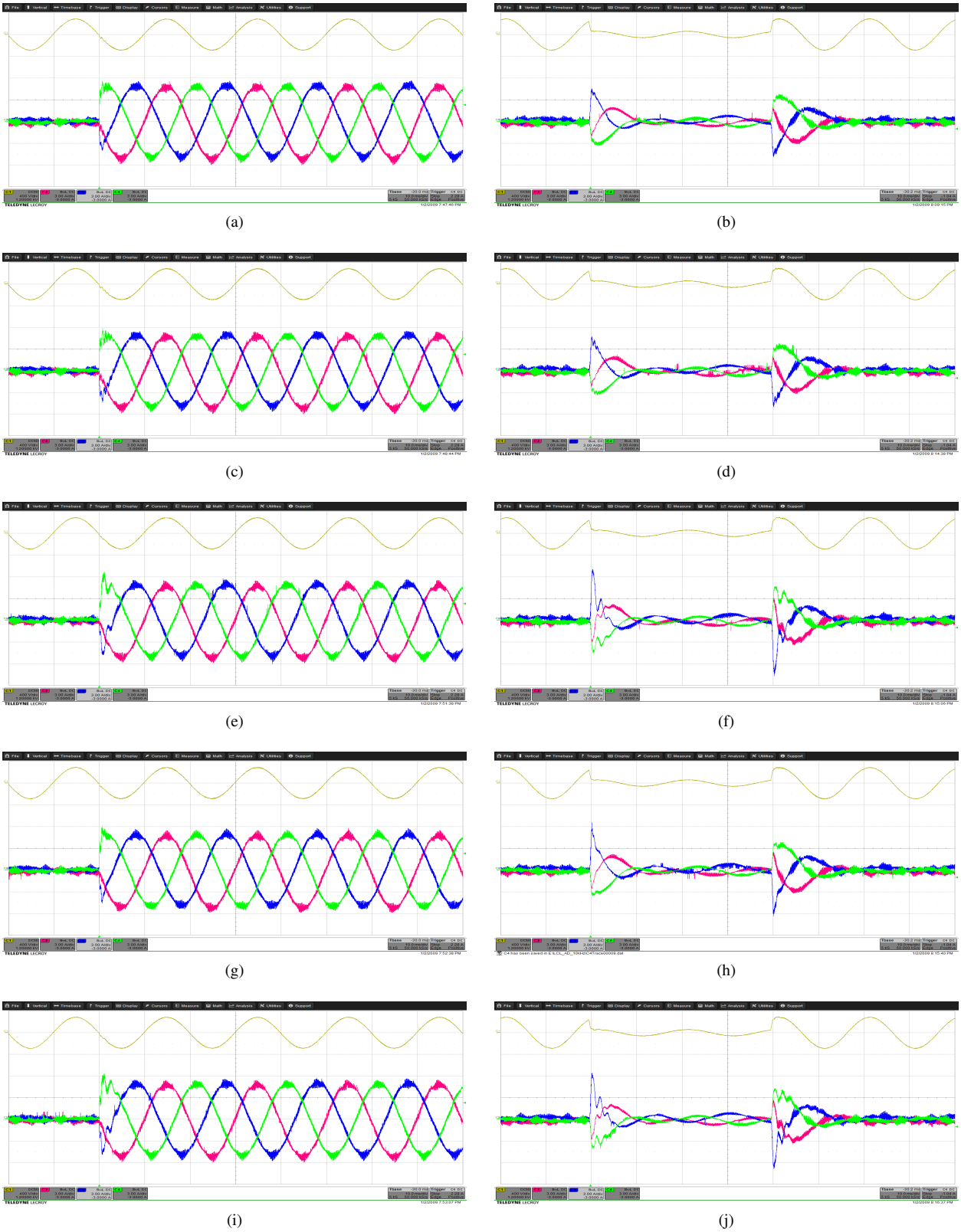

Fig. 10: Reference tracking and disturbance rejection test of the current controllers for the implementation with $f_s = 10\ kHz$. The yellow curve shows $E_c(t)$, while red, green, and blue curves represent $i_c(t)$. Filtered capacitor voltage feed-forward active damping with Backward-Euler implementation (a)-(b), and with non-ideal GI implementation(c)-(d). (e)-(f) "High attenuation" tuning notch filter active damping. (g)-(h): "Robust" tuning cascaded notch filter active damping. (i)-(j): "Phase Lead" tuning cascaded notch filter active damping.

This article has been accepted for publication in a future issue of this journal, but has not been fully edited. Content may change prior to final publication. Citation information: DOI 10.1109/TPEL.2018.2856634, IEEE Transactions on Power Electronics

dips of 80% of the nominal value at point of connection, $E_c(t)$. Figs 10(a) and 10(c) show the current steps for the controllers using the filtered capacitor voltage feed-forward; as expected, the controller tracks the reference with a fast and damped transient, especially with the Backward-Euler implementation [15]. Figs 10(e), 10(i), and 10(g) show the current step for the controllers using the cascade notch filters, where more oscillatory responses are obtained, which has been expected from the theoretical analysis [see Figs. 5(d), 6(c)]. Similar observations are drawn from the grid voltage step tests.

The tests have also been carried out for an implementation with switching frequency, $f_s = 7.5\ kHz$, in order to tests the validity of the theoretical analysis for different switching frequencies: the LCL filter resonance is placed at $\omega_{lcl} = \omega_s/6$. The results are shown in Fig. 11. The control parameters, for the different current control implementations, have been re-calculated for the specific switching frequency, following the same design guidelines of Section III. Overall, a reliable operation is also obtained with both implementations, which proves the suitability of both active damping strategies when the grid conditions are known. Both current and output voltage steps, with the different current controller implementations, show identical responses than the ones shown in Fig. 10.

During the case of a increment of L_e (i.e., weak grid condition), it has been also experimentally verified that the capacitor voltage feed-forward active damping action is more reliable with the Backward-Euler (or alternatively with a highly-damped GI) implementation than the case with an un-damped GI based derivative filter [cf. Figs. 11(a)-11(b) vs Figs. 11(c)-11(d)].

In order to test this feature, the system with the filtered capacitor voltage feed-forward has been driven close to instability by increasing k_{ad} considerably, as shown in Fig. 12(a) (it has been shown in [15] that k_{ad} has a great impact in the stability, and a poor tuning can easily place the dominant poles of $S_{vd}(j\omega)$ close to the stable region). Then, L_e has been increased from 0 to 0.08 p.u. and the test is repeated. The results of in Fig. 12(b) show how the system is now stabilized under weak grid conditions. This procedure has been found infeasible with the notch filter implementation.

The shape of the converter admittance serves to assess the disturbance rejection and harmonic distortion capability. Subsequently, $Y(j\omega)$ measurements in the frequency domain are provided. The procedure to measure $Y(j\omega)$ are inspired in the EN-50388 normative [38]: i) for each point, the voltage harmonic components are programmed at $E_c(t)$ and their Fast Fourier Transform (FFT) are performed (magnitude and phase); ii) the converter control is activated with $i_c(t) = 0$ and its steady state is reached quickly; then the FFT for $i_c(t)$ (magnitude and phase) is also performed; iii) $Y(j\omega)$ and $Y_g(j\omega)$ are calculated as

$$Y(j\omega) = \frac{|i_c(j\omega)|^{\text{FFT}}}{|E_c(j\omega)|^{\text{FFT}}}[\angle\phi^{\text{FFT}}_{i_c(j\omega)} - \angle\phi^{\text{FFT}}_{E_c(j\omega)}]. \qquad (22)$$

The measured converter admittances are shown in Fig. 13, which are in a good agreement with the theoretical expressions. The converter operation with the "high attenuation" and "phase lead" tunings, for the notch filter implementation, presents a region with poor harmonic rejection (i.e., a resonant peak), due to the low damping used in the filter design. On the other hand, the implementation based on the capacitor voltage feed-forward with Backward-Euler approximation shows a smooth harmonic rejection capability around ω_{res}.

The converter admittance can be used to assess the harmonic stability of the PCUs in parallel converter applications. The impedance/admittance stability criterion, employed in this work, is suitable for this kind of studies, since individual converter admittances can be lumped in an equivalent grid admittance for the stability assessment [39], [40]. Here, it is also reasonable to conclude that the capacitor voltage feed-forward is a more convenient solution for application with parallel PCUs.

Fig. 14 shows the harmonic spectrum of converter $i_c(t)$ for different current controllers. The damping approaches effectively damp the LCL harmonic resonance around ω_{res}. The converter currents have an associated THD below 1%. Also, it is important to remark that, the system with cascade notch filter has a higher harmonic content in the range of frequencies between $\omega_s/20$ and $\omega_s/10$, this can be expected from Figs. 7(a) and 6(a) where $Ynf-HA(z)$ and $Y_{nf-R}(z)$ magnitudes are bigger than $Y_{vd-B}(z)$.

VI. Conclusions

This paper presents an original comparison between two common active damping approaches for current controlled LCL grid-connected converters: 1) filtered capacitor voltage feed-forward and 2) notch filters in cascade with the main current controller. The impedance/admittance stability formulation has been used for the design of the current controller, while effectively damping the LCL filter resonance. Analytical expressions, as a function of the parameter of the system, are derived for the calculation of the converter admittance.

The laboratory scale prototype has been modelled for the theoretical analysis, which predicts an overall higher performance for the active damping technique based on the filtered capacitor voltage feed-forward. The findings of the assessment has been summarised in Table II. Significantly important is the higher robustness achieved by the controller using the capacitor voltage feed-forward, under weak grid conditions: in this situation, the system increases its stability margin, rather decreases it, which is normally expected once the current controller has been tuned for a system with different parameters.

Experimental tests have been carried out in a laboratory scaled prototype, which includes, current reference step change, response in the presence of grid faults, evaluation in weak grid conditions, and grid harmonics injection for converter admittance measurement. The experimental results fully verify the theoretical analysis.

Finally, it is worth mentioning the suitability of the impedance/admittance stability criterion, employed in this work to address the paralleling of inverters. The superiority of the capacitor voltage feed-forward technique would suggest this technique as the one most suitable in order to reduce converters' interactions and stability issues in ac microgrids.

This article has been accepted for publication in a future issue of this journal, but has not been fully edited. Content may change prior to final publication. Citation information: DOI 10.1109/TPEL.2018.2856634, IEEE Transactions on Power Electronics

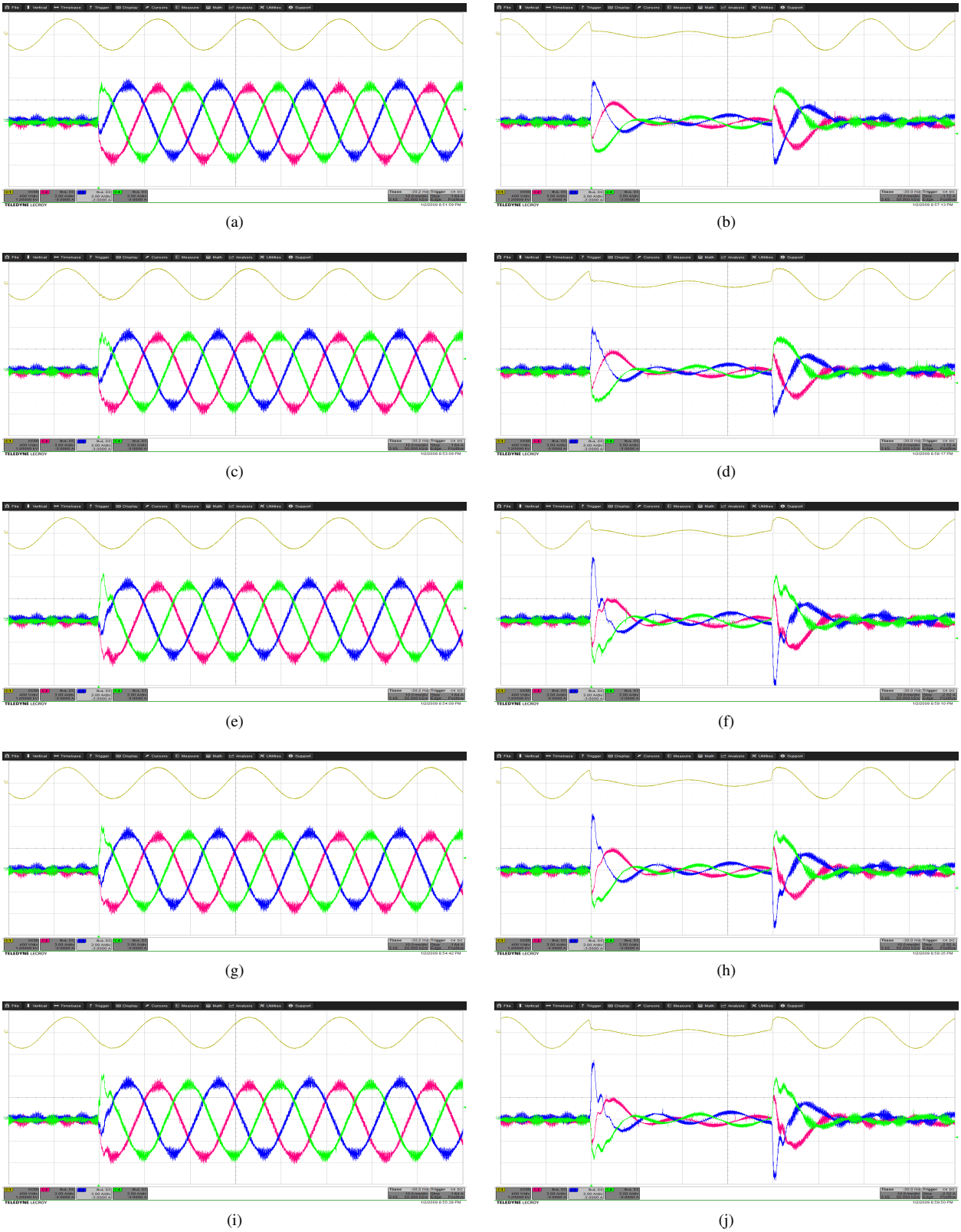

(a) (b) (c) (d) (e) (f) (g) (h) (i) (j)

Fig. 11: Reference tracking and disturbance rejection test of the current controllers for the implementation with $f_s = 7.5\ kHz$. The yellow curve shows $E_c(t)$, while red, green, and blue curves represent $i_c(t)$. Filtered capacitor voltage feed-forward active damping with Backward-Euler implementation (a)-(b), and with non-ideal un-damped GI implementation (c)-(d). (e)-(f) "High attenuation" tuning notch filter active damping. (g)-(h): "Robust" tuning cascaded notch filter active damping. (i)-(j): "Phase Lead" tuning cascaded notch filter active damping.

This article has been accepted for publication in a future issue of this journal, but has not been fully edited. Content may change prior to final publication. Citation information: DOI 10.1109/TPEL.2018.2856634, IEEE Transactions on Power Electronics

Table II: summary of the comparison.

	Notch filter	Capacitor voltage feedforward
Disturbance Rejection	Worse at frequencies around $\omega_s/10$.	Good.
Converter Admittance	Low disturbance rejection peaks with very low ξ_z.	Predicted passive behaviour up to $\omega_s/3$.
Dynamic Response	Fast and damped.	Fast and damped.
Robustness at Nominal Conditions	Slightly lower (”robust” design).	High.
Resonant Frequency Drifts	Not very sensitive if taken into account in the design stage.	Not sensitive.
Weak Grid Conditions	Dynamic response and stability worsens.	Stability not compromised.

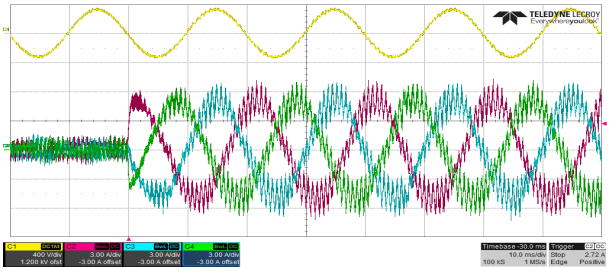

(a)

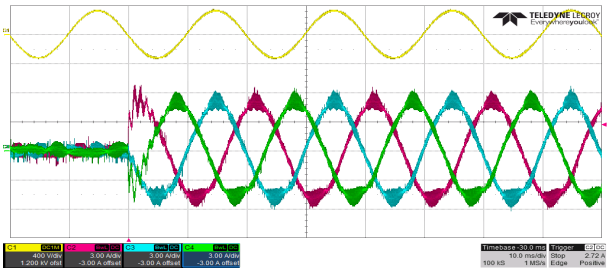

(b)

Fig. 12: Reference tracking of current controller with filtered capacitor voltage feed-forward action, $k_p = 57.33$ and $k_{ad} = 44$ (a): System with normal grid conditions $L_e = 0$, (b): System with weak grid conditions $L_e = 0.08\ p.u.$, $k_p = 57.33$ and $k_{ad} = 44$.

REFERENCES

[1] K. Astrom and T. Hagglund, *PID Controllers: Theory , Design and Tuning, Second Edition*. Instrument Society of America, 1995, pp. 274–279.

[2] F. Shinskey, B. Liptak, R. Bars, and J. Hetthessy, “2.6 Control Systems–Cascade Loops,” in *Process Control and Optimization, Volume II*. ISA, Taylor Francis, 2006, pp. 148–156.

[3] A. Vidal, F. D. Freijedo, A. G. Yepes, P. Fernandez-Comesana, J. Malvar, O. Lopez, and J. Doval-Gandoy, “Assessment and optimization of the transient response of proportional-resonant current controllers for distributed power generation systems,” *IEEE Trans. Ind. Electron.*, vol. 60, no. 4, pp. 1367–1383, Apr. 2013.

[4] A. Timbus, M. Liserre, R. Teodorescu, P. Rodriguez, and F. Blaabjerg, “Evaluation of current controllers for distributed power generation systems,” *IEEE Trans. Power Electron.*, vol. 24, no. 3, pp. 654–664, 2009.

[5] J. Dannehl, F. Fuchs, S. Hansen, and P. Thogersen, “Investigation of active damping approaches for pi-based current control of grid-connected pulse width modulation converters with LCL filters,” *IEEE Trans. Ind. Appl.*, vol. 46, no. 4, pp. 1509–1517, 2010.

[6] G. Gohil, L. Bede, R. Teodorescu, T. Kerekes, and F. Blaabjerg, “Line filter design of parallel interleaved vscs for high-power wind energy conversion systems,” *IEEE Trans. Power Electron.*, vol. 30, no. 12, pp. 6775–6790, 2015.

[7] L. Harnefors, A. G. Yepes, A. Vidal, and J. Doval-Gandoy, “Passivity-based stabilization of resonant current controllers with consideration of time delay,” *IEEE Trans. Power Electron.*, vol. 29, no. 12, pp. 6260–6263, 2014.

[8] R. Pena-Alzola, M. Liserre, F. Blaabjerg, R. Sebastian, J. Dannehl, and F. Fuchs, “Analysis of the passive damping losses in LCL-filter-based grid converters,” *IEEE Trans. Power Electron.*, vol. 28, no. 6, pp. 2642–2646, 2013.

[9] R. Pena-Alzola, M. Liserre, F. Blaabjerg, M. Ordonez, and Y. Yang, “LCL-filter design for robust active damping in grid-connected converters,” *IEEE Trans. Ind. Informat.*, vol. 10, no. 4, pp. 2192–2203, 2014.

[10] S. Parker, B. McGrath, and D. Holmes, “Regions of active damping control for LCL filters,” *IEEE Trans. Ind. Appl.*, vol. 50, no. 1, pp. 424–432, 2014.

[11] D. Yang, X. Ruan, and H. Wu, “Impedance shaping of the grid-connected inverter with LCL filter to improve its adaptability to the weak grid condition,” *IEEE Trans. Power Electron.*, vol. 29, no. 11, pp. 5795–5805, 2014.

[12] J. Wang, J. Yan, and L. Jiang, “Pseudo-derivative-feedback current control for three-phase grid-connected inverters with LCl filters,” *IEEE Trans. Power Electron.*, vol. 31, no. 5, pp. 3898–3912, 2016.

[13] R. Pena-Alzola, M. Liserre, F. Blaabjerg, R. Sebastian, J. Dannehl, and F. W. Fuchs, “Systematic Design of the Lead-Lag Network Method for Active Damping in LCL-Filter Based Three Phase Converters,” *IEEE Trans. Ind. Informatics*, vol. 10, no. 1, pp. 43–52, feb 2014.

[14] L. Harnefors, A. G. Yepes, A. Vidal, and J. Doval-Gandoy, “Passivity-based controller design of grid-connected vscs for prevention of electrical resonance instability,” *IEEE Trans. Ind. Electron.*, vol. 62, no. 2, pp. 702–710, 2015.

[15] F. D. Freijedo, E. Rodriguez-Diaz, M. S. Golsorkhi, J. C. Vasquez, and J. M. Guerrero, “A Root-Locus Design Methodology Derived from the Impedance/Admittance Stability Formulation and Its Application for LCL Grid-Connected Converters in Wind Turbines,” *IEEE Trans. Power Electron.*, vol. 8993, no. c, pp. 1–1, 2017.

[16] Z. Xin, P. Loh, X. Wang, F. Blaabjerg, and Y. Tang, “Highly accurate derivatives for LCl-filtered grid converter with capacitor voltage active damping,” *IEEE Trans. Power Electron.*, vol. 31, no. 5, pp. 3612–3625, 2016.

[17] M. Malinowski and S. Bernet, “A Simple Voltage Sensorless Active Damping Scheme for Three-Phase PWM Converters With an LCL Filter,” *IEEE Trans. Ind. Electron.*, vol. 55, no. 4, pp. 1876–1880, apr 2008.

[18] M. H. Bierhoff and F. W. Fuchs, “Active damping for three-phase PWM rectifiers with high-order line-side filters,” *IEEE Trans. Ind. Electron.*, vol. 56, no. 2, pp. 371–379, 2009.

This article has been accepted for publication in a future issue of this journal, but has not been fully edited. Content may change prior to final publication. Citation information: DOI 10.1109/TPEL.2018.2856634, IEEE Transactions on Power Electronics

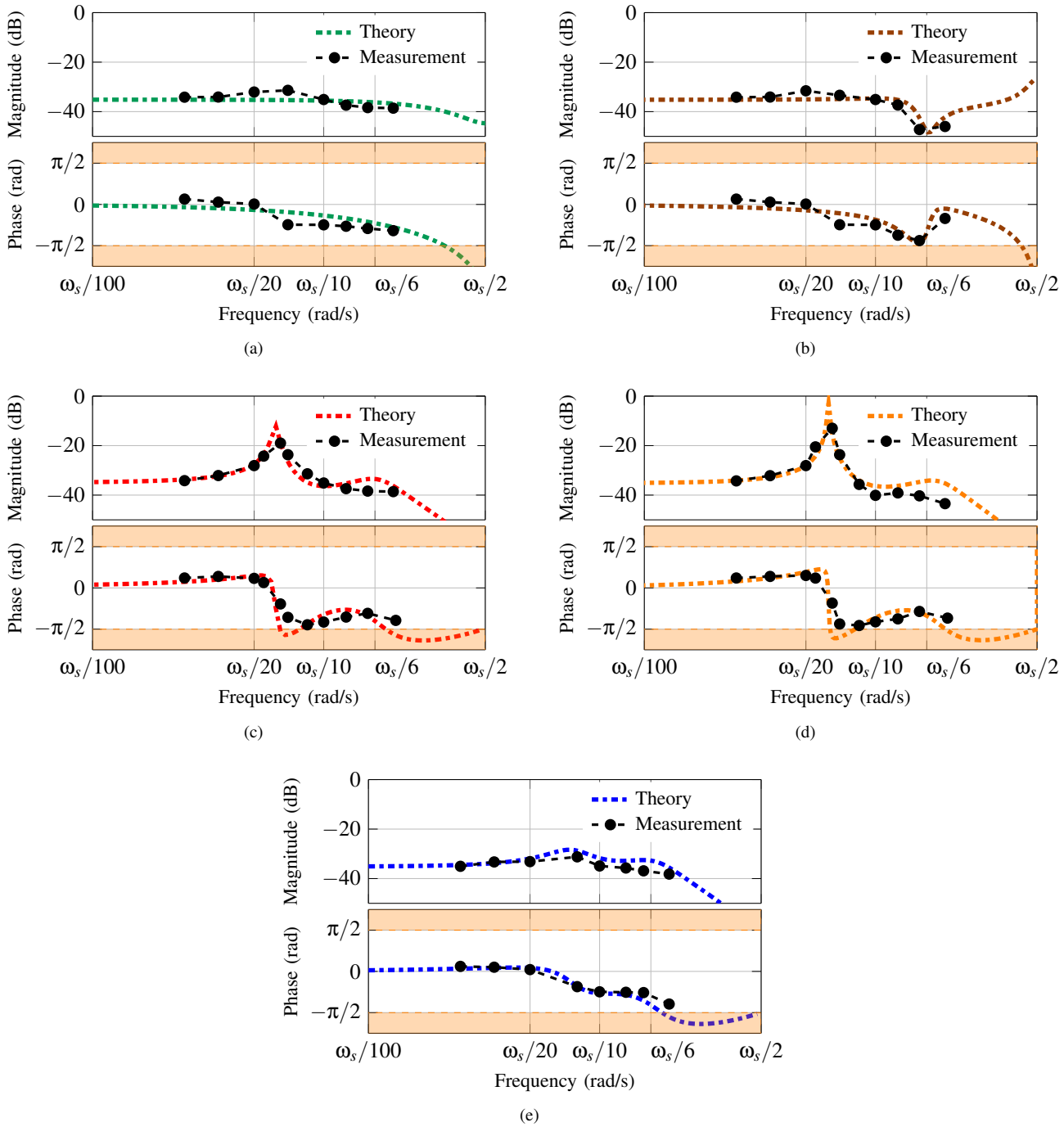

Fig. 13: $Yc(\omega)$ measurement test. (a): $Y_{vd-B}(\omega)$. (b): $Y_{vd-NIGI}(\omega)$. (c): $Y_{nf-HA}(\omega)$. (d): $Y_{nf-PL}(\omega)$. (e): $Y_{nf-R}(\omega)$.

[19] V. Blasko and V. Kaura, "A novel control to actively damp resonance in input LC filter of a three-phase voltage source converter," *IEEE Trans. Ind. Appl.*, vol. 33, no. 2, pp. 542–550, 1997.

[20] W. Wu, Y. Li, Y. He, H. S.-H. Chung, M. Liserre, and F. Blaabjerg, "Damping Methods for Resonances Caused by LCL-filter-based Current-controlled Grid-tied Power Inverters: an Overview," *IEEE Trans. Ind. Electron.*, vol. 46, no. c, pp. 1–1, 2017.

[21] J. Dannehl, M. Liserre, and F. Fuchs, "Filter-based active damping of voltage source converters with LCL filter," *IEEE Trans. Ind. Electron.*, vol. 58, no. 8, pp. 3623–3633, 2011.

[22] W. Yao, Y. Yang, X. Zhang, F. Blaabjerg, and P. C. Loh, "Design and Analysis of Robust Active Damping for LCL Filters Using Digital Notch Filters," *IEEE Trans. Power Electron.*, vol. 32, no. 3, pp. 2360–2375, mar 2017.

[23] R. Pena-Alzola, J. Roldan Perez, E. Bueno, F. Huerta, D. Campos-Gaona, M. Liserre GAE, and G. M. Burt, "Robust Active Damping in LCL-filter based Medium-Voltage Parallel Grid-Inverters for Wind Turbines," *IEEE Transactions on Power Electronics*, vol. 8993, no. c, pp. 1–1, 2018.

[24] M. Liserre, A. Dell'Aquila, and F. Blaabjerg, "Genetic Algorithm-Based Design of the Active Damping for an LCL-Filter Three-Phase Active Rectifier," *IEEE Trans. Power Electron.*, vol. 19, no. 1, pp. 76–86, jan 2004.

[25] R. Pena-Alzola, M. Liserre, F. Blaabjerg, M. Ordonez, and T. Kerekes, "A Self-commissioning Notch Filter for Active Damping in a Three-Phase LCL -Filter-Based Grid-Tie Converter," *IEEE Trans. Power Electron.*, vol. 29, no. 12, pp. 6754–6761, dec 2014.

[26] N. Strachan and D. Jovcic, "Stability of a variable-speed permanent

This article has been accepted for publication in a future issue of this journal, but has not been fully edited. Content may change prior to final publication. Citation information: DOI 10.1109/TPEL.2018.2856634, IEEE Transactions on Power Electronics

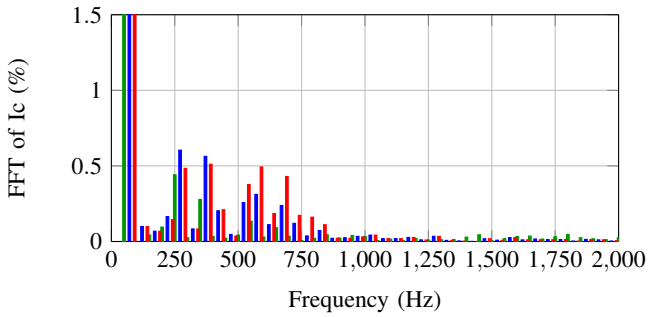

(a)

Fig. 14: FFT Analysis of $i_c(t)$ for the current controllers, using filtered capacitor voltage feed-forward (green), and cascade notch filters with the "high attenuation" (red) and "robust" (blue) tuning

magnet wind generator with weak AC grids," *IEEE Trans. Power Del.*, vol. 25, no. 4, pp. 2779–2788, 2010.

[27] L. Harnefors, L. Zhang, and M. Bongiorno, "Frequency-domain passivity-based current controller design," *IET Power Electron.*, vol. 1, no. 1, pp. 455–465, 2008.

[28] F. D. Freijedo, D. Dujic, and J. A. Marrero-Sosa, "Design for passivity in the z-domain for LCL grid-connected converters," in *Proc. of the IEEE Industrial Electronics Society Annual Conference*, Firenze, Italy, Oct. 2016, pp. 7016–7021.

[29] G. C. Goodwin, S. F. Graebe, and M. E. Salgado, *Control System Design*. Prentice Hall, 2000, pp. 80–81, 98–99, 178–189, 594–597, 603–608.

[30] L. Harnefors, "Modeling of three-phase dynamic systems using complex transfer functions and transfer matrices," *IEEE Trans. Ind. Electron.*, vol. 54, no. 4, pp. 2239–2248, Aug. 2007.

[31] M. Cespedes and J. Sun, "Impedance modeling and analysis of grid-connected voltage-source converters," *IEEE Trans. Power Electron.*, vol. 29, no. 3, pp. 1254–1261, 2014.

[32] B. Wen, D. Boroyevich, R. Burgos, P. Mattavelli, and Z. Shen, "Analysis of d-q small-signal impedance of grid-tied inverters," *IEEE Trans. Power Electron.*, vol. 31, no. 1, pp. 675–687, 2016.

[33] B. Wen, D. Dong, D. Boroyevich, R. Burgos, P. Mattavelli, and Z. Shen, "Impedance-based analysis of grid-synchronization stability for three-phase paralleled converters," *IEEE Trans. Power Electron.*, vol. 31, no. 1, pp. 26–38, 2016.

[34] R. C. Dorf and R. H. Bishop, *Modern Control Systems*. Prentice Hall, 2007.

[35] S. Bhattacharyya, H. Chapellat, and L. Keel, *Robust control: the parametric approach*. Prentice-Hall, 1995.

[36] L. Harnefors, R. Finger, X. Wang, H. Bai, and F. Blaabjerg, "VSC Input-Admittance Modeling and Analysis Above the Nyquist Frequency for Passivity-Based Stability Assessment," *IEEE Trans. Ind. Electron.*, vol. 64, no. 8, pp. 6362–6370, aug 2017.

[37] E. Mollerstedt and B. Bernhardsson, "Out of control because of harmonics-an analysis of the harmonic response of an inverter locomotive," *IEEE Control Syst. Mag.*, vol. 20, no. 4, pp. 70–81, 2000.

[38] *EN50388. Railway Applications – Power supply and rolling stock – Technical criteria for the coordination between power supply (substation) and rolling stock to achieve interoperability*, Cenelec Std., 2012.

[39] J. L. Agorreta, M. Borrega, J. López, and L. Marroyo, "Modeling and control of N-paralleled grid-connected inverters with LCL filter coupled due to grid impedance in PV plants," *IEEE Transactions on Power Electronics*, vol. 26, no. 3, pp. 770–785, 2011.

[40] F. Wang, J. L. Duarte, M. A. M. Hendrix, and P. F. Ribeiro, "Modeling and Analysis of Grid Harmonic Distortion Impact of Aggregated DG Inverters," *IEEE Transactions on Power Electronics*, vol. 26, no. 3, pp. 786–797, mar 2011.

Enrique Rodriguez (S'15-M'18) received the B.Sc. and Msc degrees in Electronics Engineering at the University of Oviedo, Oviedo, Spain, in 2012 and 2014,respectively. He obtained his PhD degree in Power Electronics from Aalborg Universitet, Denmark, in 2018, where currently is a Postdoctoral Researcher. In 2017, he was a guest researcher at the Power Electronic Laboratory at EPFL. He is a member of the International Electrotechnical Commission System Evaluation Group SEG4. His research interests include DC distribution systems, control of power converters and microgrids.

Francisco D. Freijedo (M'07-SM'16) received the M.Sc. degree in physics from the University of Santiago de Compostela, Santiago de Compostela, Spain, in 2002 and the Ph.D. degree in Electrical Engineering from the University of Vigo, Vigo, Spain, in 2009. From 2005 to 2011, he was a Lecturer in the Department of Electronics Technology, University of Vigo. From 2011 to 2014, he worked in Gamesa Innovation and Technology as a Power Electronics Control Engineer, where he was involved in Wind Energy projects. From 2014 to 2016, he was a Postdoctoral Researcher in the Department of Energy Technology, Aalborg University. Since 2016, he is a Scientific Collaborator of the Power Electronics Laboratory, Ecole Polytechnique Federale de Lausanne. His research interests include many power conversion technologies and challenging control problems.

Juan C. Vasquez (M'12-SM'14) received the B.S. degree in electronics engineering from the Autonomous University of Manizales, Manizales, Colombia, and the Ph.D. degree in automatic control, robotics, and computer vision from the Technical University of Catalonia, Barcelona, Spain, in 2004 and 2009, respectively. He was with the Autonomous University of Manizales working as a teaching assistant and the Technical University of Catalonia as a Post-Doctoral Assistant in 2005 and 2008 respectively. In 2011, He was Assistant Professor and from 2014 he is working as an Associate Professor at the Department of Energy Technology, Aalborg University, Denmark where he is the Vice Programme Leader of the Microgrids Research Program. He was a Visiting Scholar at the Center of Power Electronics Systems (CPES) at Virginia Tech and a visiting professor at Ritsumeikan University, Japan. In 2017, Dr. Vasquez was awarded as Highly Cited Researcher by Thomson Reuters. His current research interests include operation, advanced hierarchical and cooperative control, optimization and energy management applied to AC/DC Microgrids, maritime microgrids, and the integration of Internet of Things into the SmartGrid.

Josep M. Guerrero (S'01-M'04-SM'08-F'15) received the B.S. degree in telecommunications engineering, the M.S. degree in electronics engineering, and the Ph.D. degree in power electronics from the Technical University of Catalonia, Barcelona, in 1997, 2000 and 2003, respectively. Since 2011, he has been a Full Professor with the Department of Energy Technology, Aalborg University, Denmark, where he is responsible for the Microgrid Research Program. From 2012 he is a guest Professor at the Chinese Academy of Science and the Nanjing University of Aeronautics and Astronautics; and from 2014 he is chair Professor in Shandong University. His research interests is oriented to different microgrid aspects, including distributed energy-storage systems, hierarchical control, energy management systems, and optimization of microgrids and islanded minigrids. In 2014 he was awarded by Thomson Reuters as ISI Highly Cited Researcher, and in 2015 same year he was elevated as IEEE Fellow for contributions to "distributed power systems and microgrids". Dr. Guerrero is an Editor for several journals. He was the Chair of the Renewable Energy Systems Technical Committee of the IEEE Industrial Electronics Society. He was the recipient of the best paper award of the IEEE TRANSACTIONS ON ENERGY CONVERSION for the period 20142015, the best paper prize of IEEE-PES in 2015, the best paper award of the Journal of Power Electronics in 2016.